PNAS RESEARCH ARTICLE | APPLIED PHYSICAL SCIENCES OPEN ACCESS

Scattering evidence of positional charge correlations in polyelectrolyte complexes

Yan N. Fang[a,b,1], Artem M. Rumyantsev[a,c,1], Angelika E. Neitzel[a,b,d], Heyi Liang[a], William T. Heller[e], Paul F. Nealey[a,b], Matthew V. Tirrell[a,b,2], and Juan J. de Pablo[a,b,2]

Edited by Glenn Fredrickson, University of California, Santa Barbara, CA; received February 10, 2023; accepted May 30, 2023

Polyelectrolyte complexation plays an important role in materials science and biology. The internal structure of the resultant polyelectrolyte complex (PEC) phase dictates properties such as physical state, response to external stimuli, and dynamics. Small-angle scattering experiments with X-rays and neutrons have revealed structural similarities between PECs and semidilute solutions of neutral polymers, where the total scattering function exhibits an Ornstein–Zernike form. In spite of consensus among different theoretical predictions, the existence of positional correlations between polyanion and polycation charges has not been confirmed experimentally. Here, we present small-angle neutron scattering profiles where the polycation scattering length density is matched to that of the solvent to extract positional correlations among anionic monomers. The polyanion scattering functions exhibit a peak at the inverse polymer screening radius of Coulomb interactions, $q^* \approx 0.2$ Å^{-1}. This peak, attributed to Coulomb repulsions between the fragments of polyanions and their attractions to polycations, is even more pronounced in the calculated charge scattering function that quantifies positional correlations of all polymer charges within the PEC. Screening of electrostatic interactions by adding salt leads to the gradual disappearance of this correlation peak, and the scattering functions regain an Ornstein–Zernike form. Experimental scattering results are consistent with those calculated from the random phase approximation, a scaling analysis, and molecular simulations.

small-angle neutron scattering | polyelectrolyte complex coacervates | charge correlations | random phase approximation | deuterium labeling

Polyelectrolyte complexes (PECs) are polymer-rich phases that result from an associative phase separation upon mixing solutions of polyanions and polycations. Polymer complexation due to electrostatic attractions is considered to be one of the physical mechanisms behind the formation of biological condensates and membraneless organelles (1–3). Within some models of prebiotic evolution, polymer-dense droplets—commonly referred to as coacervates—are proposed to have provided a means for the selective uptake of chemical species and early enzymatic activity (4–6). Synthetic PECs are promising materials with wide-ranging applications, including underwater adhesion (7, 8), gene delivery (9), and separations based on nanofiltration membranes (10). Deciphering the role of polyelectrolyte complexation in biological processes, as well as design of PEC-based materials, requires development of a comprehensive understanding of the internal PEC structure, which governs physical properties such as surface tension and viscosity.

A key concept pertaining to the internal structure of symmetric PECs—composed of polyanions and polycations of identical chain lengths and charge densities—is schematically illustrated in Fig. 1. It has been suggested theoretically that (11–13)

1. Liquid PECs (i.e., polyelectrolyte complex coacervates) are structurally similar to semidilute solutions of neutral polymers;
2. There are positional correlations in the spatial arrangement of cationic and anionic "blobs" (correlation volumes). Each blob is preferentially surrounded by its oppositely charged counterpart.

In equilibrium, salt-free PECs under Θ and good solvent conditions, the size of the concentration blob (mesh size) ξ is approximately equal to that of the corresponding electrostatic blob (12, 14).

Positional correlations between oppositely charged blobs are a central element of the hypothetical picture shown in Fig. 1. As each blob is predominantly surrounded by oppositely charged neighbors, blobs experience more Coulomb attractions than Coulomb repulsions from their neighbors. For this reason, net Coulomb attractions

Significance

Stoichiometric mixtures of oppositely charged polyelectrolytes yield macroscopic polyelectrolyte complex phases that serve as models for certain aspects of intracellular organization. Positional correlations between oppositely charged electrostatic blobs are a cornerstone of a long-standing hypothesis supported by theory to rationalize the internal structure of the polyelectrolyte complex phase, the physics of attractions between polyelectrolytes, and the polyelectrolyte complex–supernatant phase equilibrium. By means of small-angle neutron scattering, we present direct experimental evidence for positional charge correlations in liquid polyelectrolyte complexes. The experimental observations are in line with theoretical predictions from the random phase approximation and molecular dynamics simulations. Collectively, our data confirm positional charge correlations as a crucial and observable feature of the polyelectrolyte complex structure.

[1]Y.N.F. and A.M.R. contributed equally to this work.

[2]To whom correspondence may be addressed. Email: mtirrell@uchicago.edu or depablo@uchicago.edu.

This article contains supporting information online at https://www.pnas.org/lookup/suppl/doi:10.1073/pnas.2302151120/-/DCSupplemental.

Published July 31, 2023.

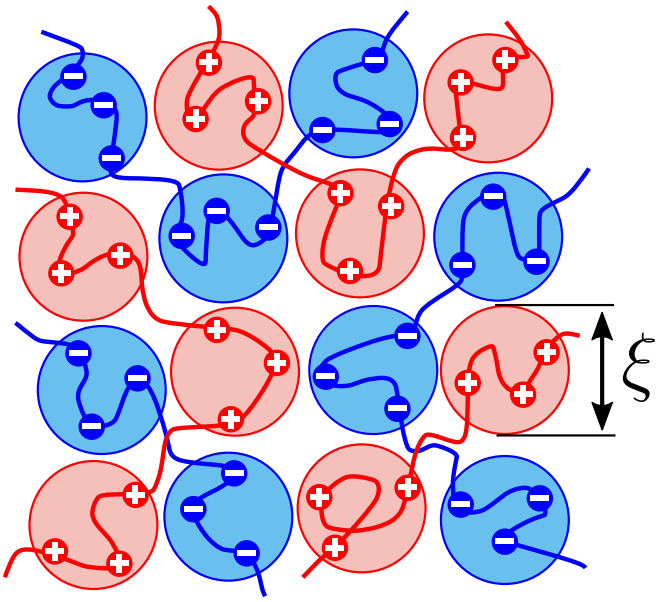

Fig. 1. Schematic representation of the internal structure of symmetric liquid PECs in a salt-free solvent. Polyanion "blobs" are mostly surrounded by polycation "blobs" due to the existence of charge correlations. These correlations are short-ranged and decay at a distance on the order of the correlation length, ξ.

between polyelectrolytes are referred to as correlation-induced. They provide the stability of the condensed PEC phase and are balanced by non-Coulomb short-range repulsions: two-body under athermal or good solvent conditions and three-body under Θ solvent conditions.

The arguments outlined above rely on a scaling approach. However, the first rigorous theoretical treatment of correlation-induced attractions between oppositely charged polyelectrolytes was developed via a field-theoretic approach. PECs cannot be adequately described at the level of a mean-field theory because the latter neglects correlations in the spatial arrangement of positively and negatively charged blobs. To overcome this shortcoming, Borue and Erukhimovich went beyond mean-field and applied the random phase approximation (RPA) to calculate the Gaussian fluctuation correction to the zero mean-field free energy (15, 16). Within the RPA, the effect of Coulomb interactions between polyelectrolyte charges on their density-density correlation functions is taken into account, thereby providing a reasonable description of the PEC phase. Advanced field-theoretic approaches, including field-theoretic simulations (FTS) (17, 18) and renormalized Gaussian fluctuation theory (RGF) (19), further support the predictions of the RPA for the structure of PECs and the charge correlations within them. We emphasize that scaling and field theory are two complementary theoretical languages that express similar physical ideas. This is demonstrated convincingly by the agreement between the analytical expressions that describe structural properties of PECs obtained from scaling arguments and the RPA (12). In the present work, we rely on both of these languages.

Small-angle scattering experiments with X-rays (SAXS) or neutrons (SANS) are commonly employed to study the internal structure of polymer systems (20), including that of PECs (21–23). To date, scattering profiles of PECs have revealed structural similarities with semidilute solutions of neutral polymers; in both cases, the resultant total scattering functions exhibit an Ornstein–Zernike (OZ) form (21)

$$G_{tot}(q) = \frac{G_{tot}(q=0)}{1+(q\xi)^{1/\nu}}, \quad [1]$$

where $1/\nu = 2$ for Θ and $1/\nu \approx 5/3$ for good solvent conditions, respectively (22–25). To the best of our knowledge, there are no reports of scattering experiments that corroborate positional charge correlations, i.e., correlations between polyanion and polycation blobs in PECs.

In what follows, we present scattering profiles that provide direct experimental evidence in support of positional charge correlations. Specifically, SANS experiments with liquid PECs made from deuterated polycations, hydrogenated polyanions, and a solvent with a scattering length density matched to that of the polycations reveal a peak at $q^{-1} \simeq \xi$. This result is consistent with a structure factor $G_{--}(q)$ arising from correlations between anionic blobs, as predicted by the RPA and coarse-grained molecular dynamics simulations. To further substantiate the argument that the observed peak originates from charge correlations, exogenous salt was added to the PEC phase, and the resultant SANS profiles were recorded. The RPA and simulations anticipate a substantial salt-induced screening of Coulomb interactions between electrostatic blobs, which leads to a gradual decrease of the correlation peak and the ultimate recovery of the OZ form for $G_{--}(q)$ at high salt concentrations. This evolution of the scattering profile is indeed observed in SANS experiments. Before presenting the experimental results, we review the relevant theory and discuss our simulation methods. Taken together, experiments, theory, and simulations provide an unambiguous confirmation of positional charge correlations in PECs.

Materials and Methods

RPA Theory of Scattering. We consider a symmetric stoichiometric PEC in a Θ solvent formed from long flexible polyelectrolytes, each containing a fraction f of ionic monomers. The monomer size is equal to a, and the Bjerrum length expressed in a units is denoted by $u = e^2/\epsilon a k_B T$, where e is the elementary charge and ϵ is the dielectric constant. All lengths are expressed in a units and all energies in units of $k_B T$. To consider charge correlations within the salt- and counterion-free PEC, we follow a procedure described elsewhere (15, 16, 26–29), and introduce the fields of polycation and polyanion densities, $\phi_+(r)$ and $\phi_-(r)$. The free energy of the PEC includes three terms

$$F_{tot}\{\phi_+(\mathbf{r});\phi_-(\mathbf{r})\} = F_{conf} + F_{el-st} + F_{vol}, \quad [2]$$

that take into account the conformational entropy of chains, Coulomb interactions, and short-range repulsions. The first term can be written in the form of the Lifshitz entropy (30)

$$F_{conf} = \frac{1}{6}\int\left[\left(\nabla\sqrt{\phi_+(\mathbf{r})}\right)^2 + \left(\nabla\sqrt{\phi_-(\mathbf{r})}\right)^2\right] d^3\mathbf{r}. \quad [3]$$

The electrostatic term is given by

$$F_{el-st} = \frac{uf^2}{2}\int \frac{(\phi_+(\mathbf{r})-\phi_-(\mathbf{r}))\,(\phi_+(\mathbf{r}')-\phi_-(\mathbf{r}'))}{|\mathbf{r}-\mathbf{r}'|} d^3\mathbf{r} d^3\mathbf{r}'. \quad [4]$$

Finally, the third contribution to the free energy is written as the leading term of a virial expansion and corresponds to three-body repulsions

$$F_{vol} = \int w\,[\phi_+(\mathbf{r})+\phi_-(\mathbf{r})]^3\, d^3\mathbf{r}. \quad [5]$$

Here, $w = C/a^6$ is the dimensionless third virial coefficient. By expanding the free energy into a series with respect to the density fluctuations, $\delta\phi_\pm(\mathbf{r}) =$

$\phi_{\pm}(\boldsymbol{r}) - \phi/2$, and applying a Fourier transform, one obtains the following elements of the inverse matrix of the structure factors

$$G^{-1}_{++}(q) = G^{-1}_{--}(q) = \frac{q^2}{6\phi} + \frac{4\pi u f^2}{q^2} + 6w\phi. \quad [6]$$

$$G^{-1}_{+-}(q) = G^{-1}_{-+}(q) = -\frac{4\pi u f^2}{q^2} + 6w\phi. \quad [7]$$

Here, ϕ is the total polymer volume fraction within the PEC phase. The first term in Eq. **7** describes the connectivity of monomers. One can also obtain it by using the Debye function for the structure factor of ideal-coiled polyelectrolytes and neglecting the translational entropy due to their substantial length, $2/\phi N g_D(x) \approx (2+x)/N\phi \approx q^2/6\phi$, where $x = Nq^2/6$ (29, 31).

At this point, it is convenient to introduce Edwards' correlation length

$$\xi_E = \left(72w\phi^2\right)^{-1/2}, \quad [8]$$

and the polymer screening radius of Coulomb interactions (15, 16).

$$r_p = \left(48\pi u f^2 \phi\right)^{-1/4}. \quad [9]$$

Inverting $G^{-1}(q)$ leads to the total structure factor of the PEC (*SI Appendix*)

$$G_{tot}(q) = 2\left(G_{++} + G_{+-}\right) = \frac{(6w\phi)^{-1}}{1 + (q\xi_E)^2}, \quad [10]$$

which corresponds to the total polymer volume fraction, $\phi(\boldsymbol{r}) = \phi_+(\boldsymbol{r}) + \phi_-(\boldsymbol{r})$, and has a simple OZ form. The respective correlation function of the total polymer density obtained via the Fourier transform,

$$G_{tot}(r) = \frac{3\phi}{\pi r}\exp\left(-\frac{r}{\xi_E}\right), \quad [11]$$

has Edwards' form (20, 30). The polymer charge structure factor (termed, for brevity, the charge structure factor) is given by

$$G_{ch}(q) = 2\left(G_{++} - G_{+-}\right) = \sqrt{\frac{3\phi}{\pi u f^2}}\,\frac{(qr_p)^2}{1 + (qr_p)^4}, \quad [12]$$

and specifies the local fluctuations of the polymer charge density. It corresponds to the order parameter $\rho(\boldsymbol{r}) = \delta\phi_+(\boldsymbol{r}) - \delta\phi_-(\boldsymbol{r})$, which describes segregation between polyanions and polycations (29). Eq. **12** shows that $G_{ch}(q)$ has a peak at $q = r_p^{-1}$, which reflects the oscillatory character of the corresponding charge–charge correlation function (15, 32)

$$G_{ch}(r) = \frac{3\phi}{\pi r}\exp\left(-\frac{r}{\sqrt{2}r_p}\right)\cos\left(\frac{r}{\sqrt{2}r_p}\right). \quad [13]$$

This peak arises due to charge correlations between oppositely charged blobs and is absent in $G_{tot}(q)$ given by Eq. **10**. Fully fluctuating field-theoretic simulations (performed for diblock polyampholytes) have also predicted the existence of this correlation peak (33).

The RPA enables calculation of the Gaussian correlation correction to the free energy (16, 26)

$$F_{corr} = \frac{1}{6\sqrt{2}\pi r_p^3}, \quad [14]$$

which is responsible for attractions between the oppositely charged polyelectrolytes. This term is absent in Eq. **2**, which defines the system's free energy at the mean-field level without fluctuations. For PECs in equilibrium with the supernatant, the density is defined by the interplay between Coulomb correlation attractions and three-body repulsions

$$\phi = 0.49u^{1/3}f^{2/3}w^{-4/9}. \quad [15]$$

Strictly speaking, this result and the entire RPA analysis are valid for $w \ll 1$, when the total density fluctuations are weak. This limitation is known for neutral semidilute solutions (30) and follows from a comparison of the Edwards fluctuation correction, $F_E = -1/12\pi\xi_E^3 = -36\sqrt{2}w^{3/2}\phi^3/\pi$, to the mean-field three-body term, $F_{vol} = w\phi^3$ (34). In contrast, at $w \gtrsim 1$, fluctuations are strong and scaling should be used instead of the RPA. We perform our analysis for $w \ll 1$ and provide a scaling interpretation at the cross-over, $w \simeq 1$, where field-theoretic and scaling results should coincide. At $w \simeq 1$, Eqs. **8**, **9**, and **15** demonstrate that the polymer screening radius of Coulomb interactions and the Edwards correlation length are both on the order of the electrostatic blob size

$$r_p \simeq \xi_E \simeq \xi_e \simeq u^{-1/3}f^{-2/3}. \quad [16]$$

This equality reflects the scaling idea that, in the regime of strong fluctuations, there is a single characteristic scale called correlation length or the blob size, which quantifies both electrostatic attractions and short-range repulsions.

As salt is added to the PEC, Coulomb interactions between the polyelectrolytes are screened. The respective Debye radius decreases with increasing salt concentration, $c_s = c_{s,+} + c_{s,-}$:

$$r_D^{-2} = 4\pi u c_s. \quad [17]$$

At the level of the RPA, the effect of added salt can be taken into account by modifying the Fourier transform from a bare to a screened Coulomb potential, $1/q^2 \to 1/(q^2 + r_D^{-2})$, in Eqs. **6** and **7**. In the presence of salt, the charge structure factor is equal to

$$G_{ch}(q) = \sqrt{\frac{3\phi}{\pi u f^2}}\,\frac{1}{\frac{1}{Q^2+s} + Q^2}, \quad [18]$$

with

$$s = \frac{r_p^2}{r_D^2} = c_s\sqrt{\frac{\pi u}{3\phi f^2}}; \qquad Q = qr_p. \quad [19]$$

Following Borue and Erukhimovich (15, 16), we have introduced the reduced wavevector Q and the parameter s defining the reduced salt concentration. For $c_s = s = 0$, Eq. **18** coincides with the salt-free charge structure factor given by Eq. **12**. The functional form of $G_{ch}(q)$ suggests that the scattering peak survives only at low salt concentrations; namely, at $s \le 1$. As c_s increases, the peak height goes down and the peak position shifts to lower wavevectors, $Q^* = \sqrt{1-s}$. At high salt concentrations, $s \ge 1$, the peak disappears. In the limit of $s \gg 1$, when all Coulomb interactions are screened by salt, $G_{ch}(q)$ has a simple OZ form. Finally, $G_{tot}(q)$, defined by Eq. **10**, remains unchanged upon addition of salt (15, 16).

The results above were obtained with the standard RPA and are sufficient to explain at a qualitative level the shape and evolution of the scattering curves obtained in experiments and simulations. Two additional modifications can be introduced to achieve quantitative agreement between theory and simulations.

First, the effect of Coulomb correlation attractions on the correlation functions and the structure factors can be taken into account by adding the respective free energy term (Gaussian fluctuation correction) to the total free energy, F_{tot} (29). This term can be calculated within the RPA and, for salt-added systems, equals (16, 26)

$$F_{corr} = \frac{(1-s)\sqrt{2-s}}{12\pi r_p^3}. \quad [20]$$

Adding this term changes the Edwards screening length

$$\xi_E^{-2} = 12\phi\left(6w\phi + \frac{d^2F_{corr}}{d\phi^2}\right), \quad [21]$$

and hence the total structure factor of the PEC

$$G_{tot}(q) = \sqrt{\frac{3\phi}{\pi u f^2}}\,\frac{1}{Q^2+t}, \quad [22]$$

while the charge structure factor remains unchanged. Here, the parameter controlling the effective solvent quality is $t = r_p^2/\xi_E^2$ (15). With this modification, the equality between the total structure factor at $q \to 0$ and the osmotic compressibility of the PEC is now satisfied, as required by thermodynamics (20, 30)

$$G_{tot}(q \to 0) = \left[\frac{d\,(\Pi_{vol} + \Pi_{corr})}{d\phi}\right]^{-1} = \left[\phi\frac{d^2\,(F_{vol} + F_{corr})}{d^2\phi}\right]^{-1}. \quad [23]$$

This result predicts a decrease in $G_{tot}(q = 0)$ for increasing salt concentrations when the polymer volume fraction in the PEC is constant. As salt is added, Coulomb attractions between polyelectrolytes become more screened while three-body repulsions are unchanged, leading to a decrease of PEC compressibility. Note that the approach adopted here to incorporate the effects of Coulomb correlation attractions is the simplest but not the most rigorous. For a stricter derivation of fluctuation-induced corrections to the correlation functions, we refer readers to the systematic perturbation analysis by Castelnovo and Joanny (35).

Second, to account for the effect of fluctuations on the charge structure factor, the Brazovskii–Fredrickson–Helfand (BFH) approximation can be used, instead of the standard RPA. The BFH approximation describes correlations in systems that may undergo order-disorder transitions (36–39). In PECs, this transition would be a microphase separation between polyanions and polycations in cases of high incompatibility. The latter can be described as short-range pairwise repulsions between polyanion and polycation monomers, $F_{rep} = \int \chi_{+-}\phi_+(\boldsymbol{r})\phi_-(\boldsymbol{r})d^3\boldsymbol{r}$, and $\rho(\boldsymbol{r})$ is the relevant order parameter (29, 39–42). Within the mean-field calculation of the correlation functions, i.e., at the RPA level, $G_{ch}(q) \propto \left(1/(Q^2 + s) + Q^2 - \alpha\chi_{+-}\right)^{-1}$ and the peak at $Q = Q^*$ in $G_{ch}(q)$ increases and diverges as the critical incompatibility is approached, $\chi_{+-}^{cr} = (2-s)/\alpha$ with $\alpha^{-1} = 2f\sqrt{\pi u/3\phi}$ (29, 39). BFH theory corrects this divergence and provides a fluctuation-induced renormalization of the charge structure factor in the disordered phase, even in the absence of polyelectrolyte incompatibility. Therefore, the charge structure factor takes the following form

$$G_{ch}(q) = \sqrt{\frac{3\phi}{\pi u f^2}}\,\frac{1}{\frac{1}{Q^2 + s} + Q^2 + R}. \quad [24]$$

When expanded into a series near the peak, Eq. **24** reduces to the conventional BFH form (38, 39), $G_{ch}^{-1} \propto 2 - s + R + 4(1-s)\,(Q - Q^*)^2$. To recapitulate, the positive values of R should be attributed to fluctuations, while negative R are possible if the chains are effectively incompatible and $\chi_{+-} > 0$ (*SI Appendix*).

Coarse-Grained Simulations. Coarse-grained simulations of PECs in Θ solvent conditions were performed using an implicit solvent. Polycations and polyanions were represented by a bead-spring model (43) each consisting of $N = 51$ beads, with a fraction $f = 1/3$ of charged beads with charge valence $z = \pm 1$. Charged beads were evenly distributed along the chain. For all PECs considered here, the polyelectrolyte concentration was kept constant and equal to that of the salt-free system. Charged beads with $z = \pm 1$ were added to represent monovalent salt ions. Nonbonded interactions between beads were described by Lennard-Jones and Coulomb potentials, with parameters for the former corresponding to a Θ solvent. Polymer beads were connected through finite-extensible nonlinear elastic (FENE) bonds. The equilibrium salt-free PEC phase was obtained in the NPT ensemble with pressure $P = 0$ representing zero osmotic pressure of polyelectrolytes in the PECs. The equilibrium polyelectrolyte concentration of the salt-free PEC was $c_p = c_{p,+} + c_{p,-} = 0.388\sigma^{-3}$. Then, different amounts of salt beads were added to the salt-free PEC, and the new PECs were equilibrated in the NVT ensemble. The salt concentration, $c_s = c_{s,+} + c_{s,-}$, was varied between 0 and $0.3\sigma^{-3}$. All simulations were performed using LAMMPS (46). Details of the simulation potentials and procedures are described in *SI Appendix*.

The structure factor of the PEC is defined by

$$G(\boldsymbol{q}) = \frac{1}{\mathcal{N}_p}\sum_{j=1}^{N_p}\sum_{k=1}^{N_p}\beta_j\beta_k\langle exp[-i\boldsymbol{q}\cdot(\boldsymbol{R}_j - \boldsymbol{R}_k)]\rangle, \quad [25]$$

where $\boldsymbol{q}$ is the scattering vector, $\mathcal{N}_p$ is the total number of polyelectrolyte beads, $\boldsymbol{R}_j$ is the position vector of the j-th bead, and β_j is the form factor of the j-th bead. The brackets $\langle\ldots\rangle$ denote a statistical average. The 3D structure factor $G(\boldsymbol{q})$ was evaluated for PECs equilibrated in the NVT ensemble by a combination of a fast Fourier transform (FFT) method (47) for $|\boldsymbol{q}| < 1.5\sigma^{-1}$ and a direct calculation for $|\boldsymbol{q}| \geq 1.5\sigma^{-1}$. The 1D structure factor, $G(q)$, was obtained by averaging $G(\boldsymbol{q})$ with the equal magnitude of the scattering vector $q = |\boldsymbol{q}|$. The total structure factor, $G_{tot}(q)$, was calculated by setting the form factor of polycation and polyanion beads (including both charged and neutral beads) to $\beta_+ = \beta_- = 1$; the polycation structure factor, $G_{++}(q)$, was calculated by setting $\beta_+ = 1$ and $\beta_- = 0$; the polymer charge structure factor, $G_{ch}(q)$, was calculated by setting $\beta_+ = 1$ and $\beta_+ = -1$.

Polyelectrolyte Synthesis and Characterization. Poly(allyl glycidyl ether-*stat*-ethylene oxide) [poly(AGE-*stat*-EO)] and poly(allyl glycidyl ether-*stat*-d_4-ethylene oxide) [poly(AGE-*stat*-d_4-EO)] were synthesized via oxyanionic copolymerization of allyl glycidyl ether (AGE) with ethylene oxide (EO) or ethylene-d_4 oxide (EO-d_4), respectively (52). Proton NMR (^{1}H NMR) spectroscopy was used to determine the number average degree of polymerization (N_n) and molar fraction of AGE comonomer (f_{AGE}) for the protonated copolymer, and the number average degree of polymerization of AGE (N_{AGE}) of the partially deuterated copolymer.

The molar mass distribution of poly(AGE-*stat*-EO) was obtained from size exclusion chromatography (SEC) with dimethylformamide (DMF) as the eluent and a refractive index (RI) detector. The absolute weight average molar mass (M_w) of poly(AGE-*stat*-d_4-EO) was determined by SEC with a tetrahydrofuran (THF) mobile phase using a multiangle laser light scattering (MALLS) detector. The copolymer dispersity ($Đ$) was calculated using data obtained from the RI rather than the MALLS detector. The oxyanionic polymerization of AGE suffers from chain transfer to monomers (51), resulting in slight tailing toward lower molar mass chains. In this case, the $Đ$ obtained from MALLS is artificially narrow as the light scattering intensity is proportional to the product of concentration and M_w, resulting in a vanishing signal for low molar mass chains. The $N_{n,total}$ and f_{AGE} for the partially deuterated copolymer could then be calculated using M_w from MALLS, $Đ$ from the RI signal, and N_{AGE} from ^{1}H NMR spectroscopy (*SI Appendix*, Figs. S5–S7).

Postpolymerization functionalization of neutral copolymers via reaction of allyl groups with sodium 3-mercapto-1-propanesulfonate or cysteamine hydrochloride in 4/1 dimethylformamide/water solution afforded homologous pairs of protonated or partially deuterated copolyanions and copolycations; the latter were subsequently oxidized with hydrogen peroxide (52). Neutral copolymer structures and molecular characteristics are summarized in Scheme 1.

Preparation of Polyelectrolyte Complexes. Samples were prepared on a 45-mL scale, distributed into 3- ×15-mL centrifuge tubes and centrifuged at 5,000 × *g* for 90 min. All samples were prepared at a charge-stoichiometric ratio and a polymer concentration of $c_{p,i}$ = 5 mg/mL (0.5 wt %). The supernatant was removed, and the PEC phases from three samples were combined by weight in a tared Hellma quartz cuvette (path length = 1 mm) for measurement. The combined mass of each PEC sample was ≈350 mg. For samples prepared with exogenous salt, sodium chloride (NaCl) was weighed into a tared 1.5-mL Eppendorf tube, the PEC sample prepared as described before, and transferred into the Eppendorf tube. The sample was then vortexed prior to transferring it into the cell. Contrast matching conditions were calculated and measured experimentally for each polyelectrolyte (*SI Appendix*, Table S2 and Fig. S11).

SANS Experiments and Data Analysis. SANS experiments were performed at the Extended Q-Range Small-Angle Neutron Scattering Diffractometer (EQ-SANS) at the Spallation Neutron Source (SNS) at Oak Ridge National Laboratory

poly(AGE$_{55}$-*stat*-EO$_{128}$)	M_n	$Đ^b$	f_{AGE}
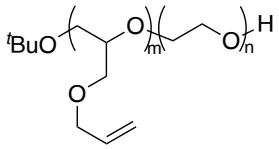	12 kg/mol[a]	1.15	0.30[a]
poly(AGE$_{64}$-*stat*-d_4-EO$_{142}$)	M_n	$Đ^b$	f_{AGE}
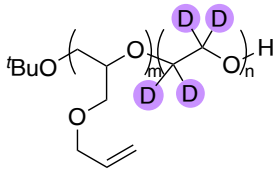	13 kg/mol[c]	1.07	0.31[c]

Scheme 1. Molecular characteristics of near-ideally random copolyelectrolyte precursors. [a]Calculated via end-group analysis using ^{1}H NMR spectroscopy. [b]Calculated from the dRI detector signal. [c]Calculated using absolute M_W from SEC-MALLS, D from the dRI detector signal, and $N_{n,AGE}$ from ^{1}H NMR spectroscopy with end-group analysis.

(ORNL) (53). To collect the SANS data presented here, two configurations of the instrument were employed: 4-m sample-to-detector distance with a wavelength band of min = 2.5 Åand 2.5-m sample-to-detector distance with min = 2.5 Å. This provided momentum transfer q, $q = 4\pi \sin(\theta)/\lambda$, from 0.01 Å^{-1} to 0.70 Å^{-1}; here, 2θ is the scattering angle and λ is the neutron wavelength. All data reduction was accomplished using the *drtsans* software (54), which performs the standard data reduction corrections such as for wavelength-dependent flux and neutron transmission, detector response, empty cell scattering, etc. We used a calibrated porous silica standard to get the scale factor to convert the measured data into absolute intensity units of 1/cm (55). The temperature was kept constant at 20.0 ± 0.1 °C using one of the standard sample environments of the instrument to make the measurement temperature identical to the temperature at which the samples were originally prepared.

Scattering profiles were obtained for 1) poly(Sulf-*stat*-EO)/poly(Am$_{0x}$-*stat*-EO) in D_2O, 2) poly(Sulf-*stat*-d_4-EO))/poly(Am$_{0x}$-*stat*-EO) matching the scattering length density (SLD) of the solvent to that of the polyanion, and 3) poly(Sulf-*stat*-EO)/poly(Am$_{0x}$-*stat*-d_4-EO) matching the SLD of the solvent to that of the polycation. These provided the experimental profiles of G_{tot}, G_{++}, and G_{--}. The signal for G_{++} was weak due to increased incoherent scattering from water, and thus, further measurements were confined to those of G_{--}. The reduced data were plotted using the Irena SAS package in IGOR Pro, and solvent backgrounds were subtracted from PEC scattering profiles. Charge structure factor profiles, $G_{ch}(q)$, were generated by overlapping the experimental $G_{--}(q)$ and $G_{tot}(q)$ profiles at high q, normalizing their values to provide twice higher values of $G_{tot}(q)$ in this q-region, and then subtracting the scattering profiles from each other according to the theoretical equation $G_{ch}(q) = 4G_{--}(q) - G_{tot}(q)$.

Results and Discussion

Choice of the Experimental System. The theoretical picture provided by the RPA and scaling analysis was developed for weakly charged PECs at equilibrium. Polyelectrolyte complexation can produce liquid- or solid-like PECs; the latter are known to be kinetically trapped structures below their glass transition temperature. To properly corroborate the theoretical picture, we chose polyelectrolytes derived from poly(allyl glycidyl ether-*stat*-ethylene oxide) [poly(AGE-*stat*-EO)], which yield polyelectrolyte complexes of liquid-like character at a charge density of $f = 0.3$. (52) Aqueous solubility at low charge density is facilitated by incorporation of EO as the neutral comonomer. AGE was chosen as the precursor to either the cationic or anionic monomer. Postpolymerization modification to polyelectrolytes from a common neutral precursor eases polymer characterization by conventional methods and produces homologous polycation/polyanion pairs, which reduces the number of variables to consider downstream. As EO is commercially available with near quantitative deuterium labeling, this platform enables the synthesis of an analogous, deuterated polycation/polyanion pair by the same synthetic methodology.

Salt-Free Polyelectrolyte Complexes. We start our analysis of charge correlations in equilibrium, salt-free PECs in a Θ solvent with results of coarse-grained simulations. The radial distribution function (RDF) of charges $G_{cb}(r)$, plotted in Fig. 2*A*, exhibits a damped oscillatory behavior. Owing to the zero average polymer charge density within the PEC phase, the charge RDF coincides with the charge–charge correlation function. The latter can be calculated within the RPA, Eq. **13**, and predicted to oscillate (15, 32). These oscillations are absent in the comparative system of disjointed charges, where charge screening has a simple Debye–Hückel form. They are a unique feature of polyelectrolyte systems, which arises from the interplay between the connectivity of charges and the long-range Coulomb

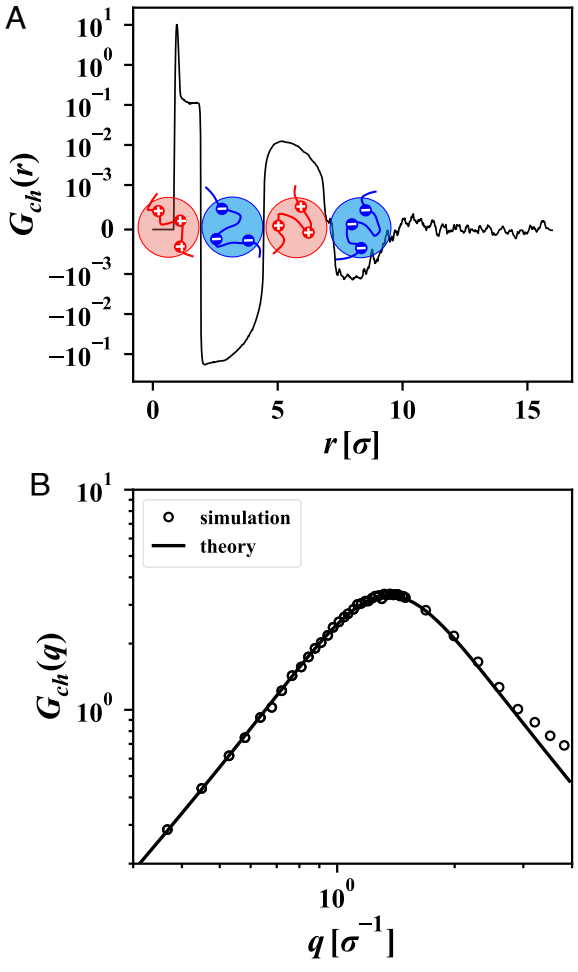

Fig. 2. (*A*) Radial distribution function of charge, $G_{ch}(r)$, and (*B*) charge structure factor, $G_{ch}(q)$, of the salt-free PEC in a Θ solvent from coarse-grained simulations. $G_{ch}(q)$ corresponds to the Fourier transform of $G_{ch}(r)$, Eq. **26**. In *A*, the *y* axis is plotted on a symmetric log scale, while in a linear scale within $(-10^{-3}, 10^{-3})$. In *B*, the solid line is the best theoretical fit for the simulation data (open circles) with the functional form given by Eq. **29**, which leads to $s \approx 0$. In the coarse-grained simulations, the chain length is $N = 51$, polyelectrolytes contain a fraction $f = 1/3$ of ionic monomers, and the Bjerrum length is set to $l_B/\sigma = 1$.

interaction potential (15, 48). The RPA shows that the period of oscillations is equal to $D = 2\sqrt{2}\pi r_p$, where r_p is the polymer screening radius of Coulomb interactions in the PEC, given by Eq. **9** (15, 32). At equilibrium, in PECs with $w \simeq 1$, the polymer screening radius is on the order of the electrostatic blob size and the concentration correlation length, $r_p \simeq \xi_e \simeq \xi$. This enables a simple scaling interpretation of the oscillations in terms of the spatial correlations of oppositely charged blobs (49), as shown schematically in Fig. 2*A*.

The periodicity of the function in real space leads to the peak at $q^* \simeq 2\pi/D$ in the Fourier representation. For undamped harmonic functions—such as in systems with long-range order—this peak has the shape of a δ-function, whereas exponential damping of oscillations is manifest in the peak's broadening and a slight shift in position. The latter is observed in the Fourier transform of the charge–charge correlation function

$$G_{ch}(q) = \frac{1}{(2\pi)^3}\int G_{ch}(\mathbf{r})e^{i\mathbf{qr}}d^3\mathbf{r}, \qquad [26]$$

which was calculated in simulations and is shown in Fig. 2*B*. The position of the correlation peak, $Q^* \ll q_m = 2\pi/\sigma$, is indicative of length scales substantially larger than the size of the monomer, σ. The monomer peak due to the covalent connectivity of beads at much higher wavevectors, q_m, is observed in simulations (*SI Appendix*, Fig. S1) and falls outside of the range of the angles probed experimentally. The charge correlation peak is theoretically anticipated within the RPA (15, 16), Eq. **12**. Introducing the dimensionless wavevector $Q = qr_p$, the theoretical functional form of the charge structure factor is predicted to be

$$G_{ch}(Q) \propto \frac{1}{\frac{1}{Q^2} + Q^2}. \qquad [27]$$

By minimizing the denominator, one can see that the peak in $G_{ch}(q)$ is expected at $Q^* = 1$, i.e., at $q^* = r_p^{-1} \simeq 1/D \simeq \xi$, in agreement with the period of oscillations in the respective charge correlation function, Eq. **13**. To recapitulate, both the RPA and coarse-grained simulations predict the existence of the scattering peak in the charge structure factor, corresponding to the existence of positional correlations between the monomers of polyanions and polycations.

Fig. 3 shows SANS profiles for "salt-free" PECs of poly($Sulf_{55}$-*stat*-EO_{128})/poly(Am_{ox55}-*stat*-EO_{128}) and poly($Sulf_{55}$-*stat*-EO_{128})/poly(Am_{ox64}-*stat*-d_4-EO_{142}) (Scheme 2) with structure factors $G_{tot}(q)$, $G_{--}(q)$, and $G_{ch}(q)$. "Salt-free" PEC refers to samples prepared without exogenous salt; hence, they contain a fraction of the counterions introduced by the polyelectrolytes. Analogous PEC samples prepared at $c_{p,i}$ = 10 mg/mL were previously shown to contain $c_{s,PEC}$ = 0.17 wt % NaCl (52). SANS samples were prepared at $c_{p,i}$ = 5 mg/mL on a scale of ca. 350 mg. It is estimated that "salt-free" PEC samples in this work contain less than 0.0017 × 350 mg = 0.6 mg NaCl as it has been shown that decreasing the $c_{p,i}$ results in denser PECs (i.e., higher $c_{p,PEC}$) that partition less salt (i.e., lower $c_{s,PEC}$) (56). The total structure factor, $G_{tot}(q)$, obtained by combining nondeuterated polyelectrolytes in D_2O, displays the expected OZ form, consistent with earlier reports (21–23) and Eq. **22**, reaffirming the structural semblance of liquid PECs and semidilute solutions of neutral polymers. A gradual slope change from −1.7 to −2 in the intermediate q-range suggests that chain conformations in the PEC phase are close to the

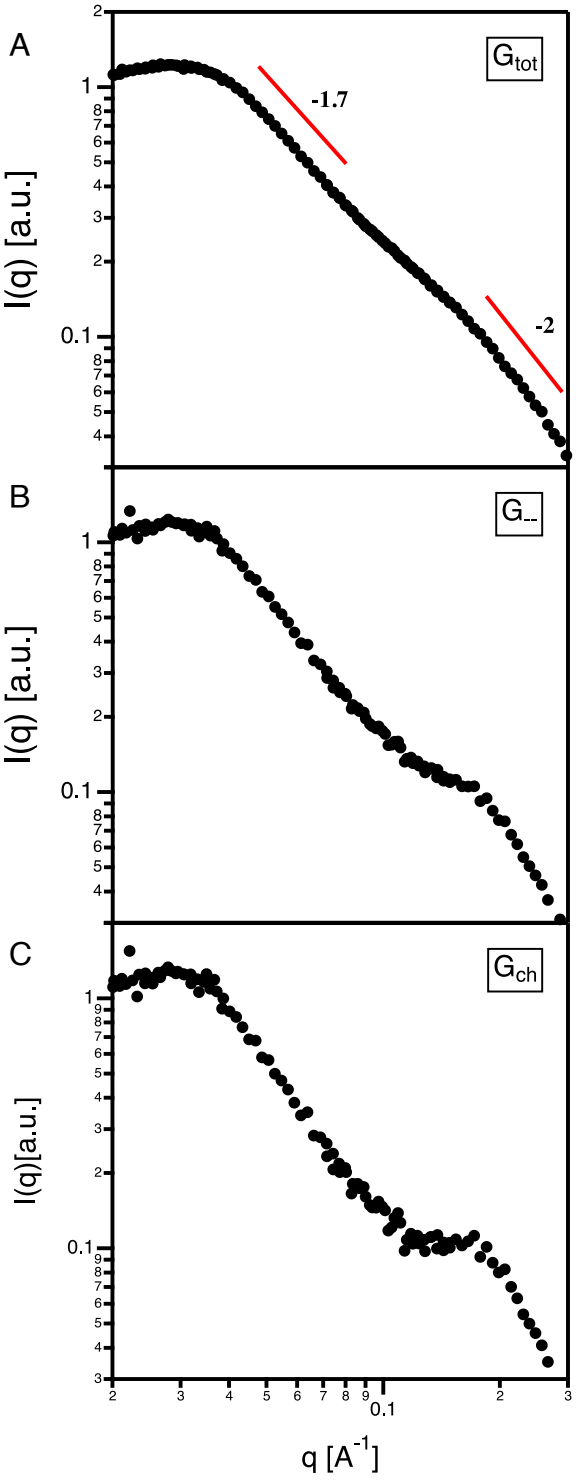

Fig. 3. Background-subtracted scattering intensity $I(q)$ as a function of the wavevector q obtained from SANS experiments with PECs of charge fraction f = 0.30 without exogenous salt. (*A*) G_{tot} is obtained via complexation of fully protonated chains of poly(Am_{ox}-*stat*-EO) and poly(Sulf-*stat*-EO) and measured against D_2O; (*B*) G_{--} is obtained via complexation of fully protonated poly(Sulf-*stat*-EO) and partially deuterated poly(Am_{ox}-*stat*-d_4-EO) and measured against H_2O/D_2O = 49/51 that contrast matches deuterated polycation; (*C*) G_{ch} is obtained by subtracting G_{tot} from G_{--} through the theoretical equation $G_{ch} = 4G_{--} - G_{tot}$ after their appropriate normalization at high q values.

cross-over between good and Θ solvent quality for PE chains, i.e., between Gaussian coil and self-avoiding walk statistics (12). The theoretical and simulation results discussed earlier were

presented for the case of Θ solvent, as the main conclusions of this work do not change when considering a good/athermal solvent. The exact RPA functional form and complimentary simulation scattering profiles for $G_{ch}(q)$ in the case of an athermal solvent are provided in *SI Appendix*.

The form of the polyanion structure factor, $G_{--}(q)$, is more complicated. A clear shoulder emerges at $q^* \approx 0.2$ Å^{-1}, which we attribute to positional charge correlations. A similar shoulder was reported in ref. 23 in solid-like PECs. The origin of the peak can be understood by considering the relationship between the different structure factors

$$G_{--}(q) = \frac{G_{tot}(q) + G_{ch}(q)}{4}. \qquad [28]$$

$G_{tot}(q)$ exhibits an OZ form that decreases monotonically, so one can argue that the shoulder in $G_{--}(q)$ can appear only due to the peak in $G_{ch}(q)$. The shoulder in $G_{--}(q)$ is seen in simulations (black curve in Fig. 5*B*), consistent with a previous report (50). We emphasize that Eq. **28** is general and independent of the type of theory used to describe scattering from PECs. It follows from the definition of the structure factors and the stoichiometry of the PEC, $\phi_+ = \phi_-$, which is provided by the experimental procedure to prepare the PECs. The resulting $G_{tot}(q)$ and $G_{--}(q)$ permits direct calculation of the charge structure factor $G_{ch}(q)$ (see experimental SANS section), which is shown in Fig. 3*C*. The correlation peak in $G_{ch}(q)$ is more evident than in $G_{--}(q)$, as is expected from the theory. The position of the peak is unchanged, $q^* \approx 0.2$ Å^{-1}, which corresponds to a polymer screening radius for Coulomb interactions equal to $r_p = 1/q^* \simeq 0.5$ nm and a period of oscillations in the charge–charge correlation function equal to $D = 2\sqrt{2}\pi r_p \approx 4.5$ nm. The latter can be viewed as an estimate of the size of the electrostatic blob.

Fitting $G_{tot}(q)$ with the OZ functional form given by Eq. **10** allows one to obtain another estimate of the blob size or, rigorously speaking, the Edwards correlation length. At $q_E = \xi_E^{-1} \approx 0.06$ Å^{-1}, the value of $G_{tot}(q)$ is half of the plateau value, which yields $\xi_E \approx 1.7$ nm. Thus, in the experiments, the polymer screening radius of Coulomb interactions and the Edwards screening length of the excluded volume interactions differ by a factor of more than three. This illustrates the approximate nature of the scaling relationship $r_p \simeq \xi_E \simeq \xi$ and the qualitative nature of the scaling arguments if applied at $w \ll 1$. In fact, the scaling approach is unable to predict the dependence of PEC density and correlation length on w (12); for this reason, it does not distinguish between r_p and ξ_E. Within the field theory, the difference between r_p and ξ_E defines the value of the parameter describing the effective solvent quality for the PEC, $t = r_p^2/\xi_E^2$, which is equal to $t \approx 0.09$ in experiments. The fact that $t \ll 1$ is consistent with theoretical expectations and estimates from simulations. Theoretically, the equilibrium density of the salt-free PEC is defined by Eq. **15**, which yields a polymer screening radius equal to $r_p = 0.34u^{-1/3}f^{-2/3}w^{1/9}$ (Eq. **9**). The Edwards correlation length is given by Eq. **21**. Using Eq. **14** for the free energy correlation term, one can find $\xi_E = 0.28u^{-1/3}f^{-2/3}w^{-1/18}$ and $t = 1.47w^{1/3}$. Since for all real polymers the dimensionless third virial coefficient is low, $w \ll 1$ (30), the value of t should be substantially lower than unity. This conclusion is also supported by our simulations where, for salt-free PECs, we used the theoretical functional forms of Eqs. **22** and **24** to fit the total and charge structure factors and found $r_p = 0.74\sigma$, $\xi_E = 1.42\sigma$, and $t = 0.27$.

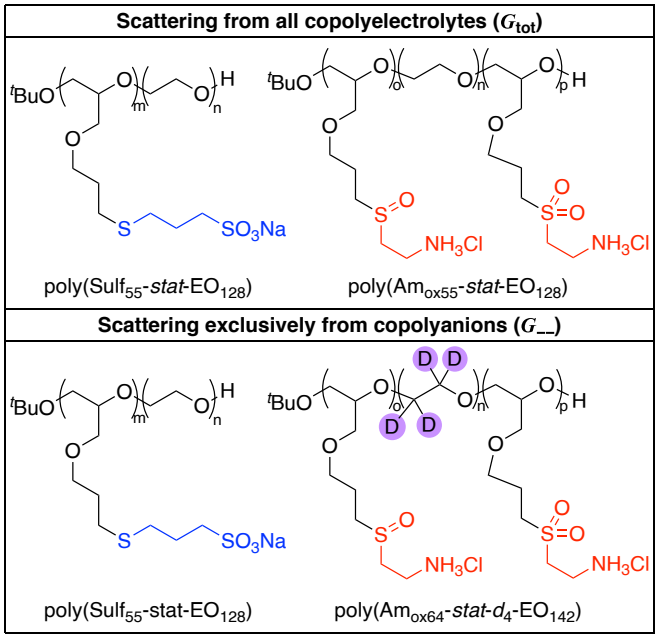

Scheme 2. Structures of near ideally random copolyelectrolytes and combinations thereof to measure the total polymer structure factor, $G_{tot}(q)$, and structure factor of polyanions, $G_{--}(q)$.

It can be seen that the experimental $G_{ch}(q)$ does not tend to zero at low q (Fig. 3*C*), contrary to what is predicted by theory and simulations. As mentioned previously, "salt-free" PECs contain a low, yet nonnegligible concentration of counterions, which screen Coulomb interactions. This implies that Eq. **27** is not exact for PECs prepared without exogenous salt. Eq. **18** with nonzero reduced concentration of salt, $s \neq 0$, should be used instead, which releases the $G_{ch}(q = 0) \to 0$ requirement. Additionally, we speculate that differences between theory and experiment arise due to deviations from ideality that are inevitable in real experimental systems. Even when polyanions and polycations are derived from an identical precursor, chemical differences between charged groups translate into polyelectrolytes with unequal SLDs. Deuterated polycations and hydrogenated polyanions were necessarily derived from different precursors and therefore do not have identical chain lengths and charge fractions (Scheme 1). Collectively, this makes Eq. **28** only approximately valid for calculations of the experimental $G_{ch}(q)$. Last, a more pronounced difference in the SLDs of hydrogenated polyanions and deuterated polycations is desirable; however, this would require full deuteration of polycations, which is synthetically challenging (Scheme 2).

Effect of Salt. To corroborate that the peak in the experimental scattering functions arises from charge correlations, we examined the effect of exogenous salt. Salt is expected to screen charge correlations and thereby lead to the gradual disappearance of the correlation peak. In order to decouple the effects of salt and polymer concentrations, the latter was fixed to that of the "salt-free" PEC, whereas the salt concentration was varied as shown with stars in Fig. 4*A*. Importantly, the salted PECs are not in equilibrium with a supernatant phase and do not coexist with it. In experiments, this was realized by adding salt to the equilibrated, "salt-free" PECs after removal of the supernatant.

With screening from increasing salt concentration, the net charge of the blobs and their Coulomb interactions decrease.

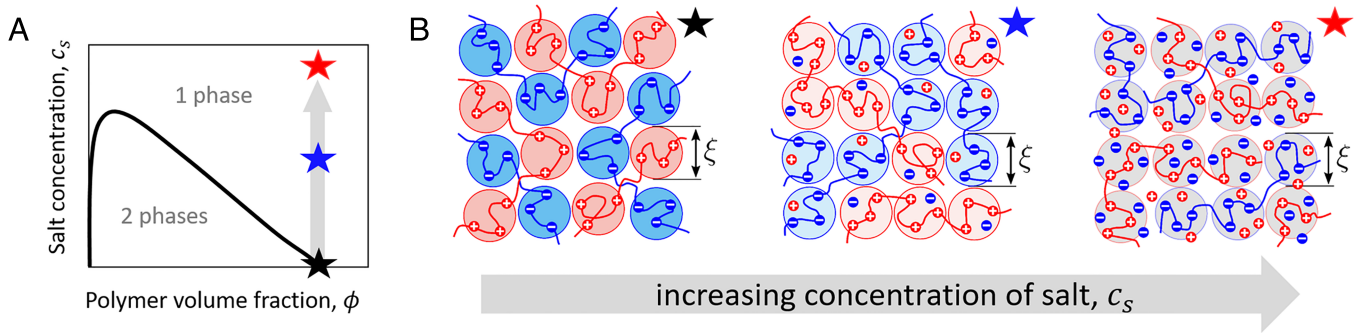

Fig. 4. (*A*) Schematic representation of the binodal phase diagram (black line) and compositions of the PECs with fixed polymer density and varying salt content (stars). (*B*) Evolution of the blob structure of the respective PECs upon addition of salt. The size of the concentration blob ξ remains unchanged owing to the constant density of the PEC.

This diminishes the extent to which the positively charged blobs are preferentially surrounded by negatively charged blobs (Fig. 4*B*, blue star). At high salt concentrations, when Coulomb interactions between the polyelectrolytes are almost entirely screened (Fig. 4*B*, red star), each blob has an equal number of polyanion and polycation blob neighbors. Charge correlations disappear and polyelectrolytes of opposite charge become effectively indistinguishable. Polyanions and polycations form interpenetrating quasi-neutral semidilute solutions, and their structure factors $G_{++}(q) = G_{--}(q)$ adopt the OZ form. Thus, when the salt concentration is sufficiently high, the $G_{--}(q)$ and $G_{ch}(q)$ peaks, which are indicative of positional charge correlations, vanish.

The same conclusions can be drawn more rigorously via analysis of the charge structure factor, which is derived theoretically and given by Eq. **24**:

$$G_{ch}(Q) \propto \frac{1}{\frac{1}{Q^2+s} + Q^2 + R}. \qquad [29]$$

Here, the dimensionless parameter $s = r_p^2/r_D^2 \propto c_s$ describes the competition between polyelectrolytes and salt ions in screening Coulomb interactions; the Debye radius due to salt, r_D, is defined by Eq. **17**. As the salt concentration increases, the peak becomes more diffuse, and its position shifts to lower wavevectors, $Q^* = \sqrt{1-s}$. Finally, at $s \geq 1$, the peak completely disappears. The predicted behavior of the charge structure factor is observed in our simulations, shown in Fig. 5. Peaks in both $G_{++}(q)$ and $G_{ch}(q)$ vanish upon the addition of salt, and at high salt concentrations, all structure factors adopt the familiar OZ form, as expected within the RPA.

To demonstrate that the agreement between theory and simulations is quantitative, we simultaneously fit the scattering profiles from simulations (dots in Fig. 5) with the respective theoretical functional forms. Namely, we use

$$G_{tot}(Q) \propto \frac{1}{Q^2+t}, \qquad [30]$$

for the total structure factor, Eq. **29** for the charge structure factor, $G_{ch}(q)$, and their combination defined by Eq. **28** for the structure factor of polycations. Theoretical results in Fig. 5 are shown with solid lines. We emphasize that only three parameters—s, t, and R—have been used to fit the entire set of scattering profiles at any salt concentration because the r_p has remained unchanged for all the curves at all c_s. Moreover, these parameters are microscopic rather than phenomenological, as they appear in the RPA theory and have a clear physical meaning (*RPA theory* section). This is supported by the dependence of the key parameter, s, which governs the evolution of the scattering profiles with addition

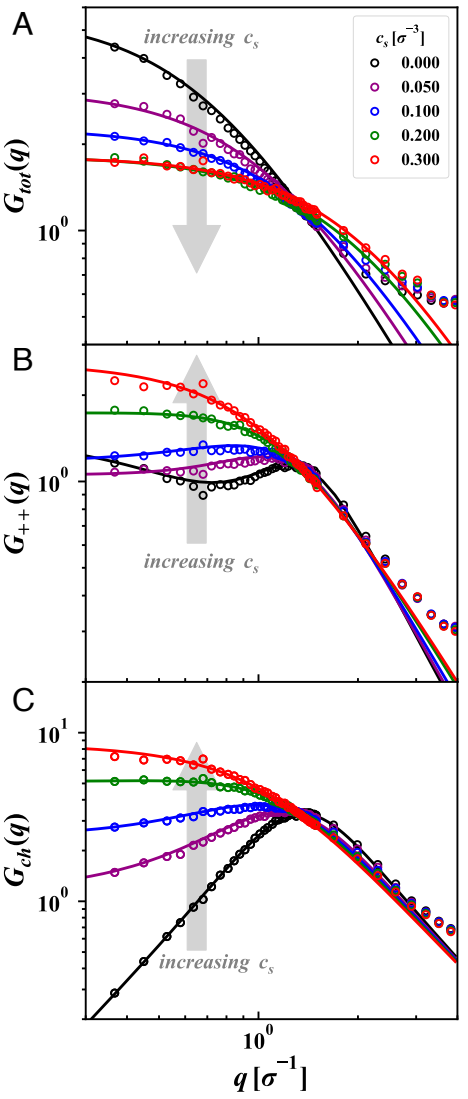

Fig. 5. Structure factor of salt-added PECs from simulations (open circles) and theory (solid lines): (*A*) total structure factor, $G_{tot}(q)$; (*B*) structure factor of polycations, $G_{++}(q)$; (*C*) charge structure factor, $G_{ch}(q)$. Simulation parameters are equal to $N = 51$, $f = 1/3$, and $l_B/\sigma = 1$. Salt concentrations are equal to $c_s\sigma^3 = 0$, 0.050, 0.100, 0.200, and 0.300. The functional forms of the theoretical fitting curves are given by Eqs. **30**, **28**, and **29**, respectively.

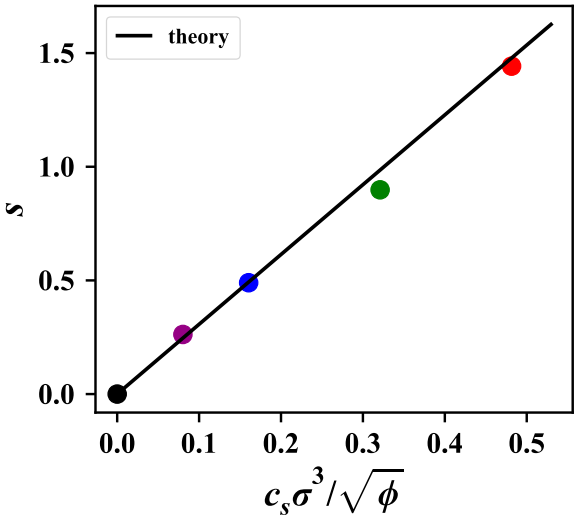

Fig. 6. Dependence of parameter s on salt concentration c_S. Dots denote the values obtained from fitting the simulation data, and the solid line shows the theoretical dependence given by Eq. **19**. In simulations, the polymer volume fraction is calculated as $\phi = c_p\sigma^3$.

of salt, on c_s. That dependence is shown in Fig. 6 and follows the theoretically expected law, Eq. **19**. Not only is it a linear dependence, but the numerical value of the slope coincides exactly with the theoretical prediction. In line with the RPA, the scattering peak disappears at s sufficiently close to unity. The resulting negative values of R (*SI Appendix*, Fig. S2) suggest an effective incompatibility between polyanions and polycations, which arises owing to the correlation-induced renormalization of short-range interactions between them and cannot be taken into account at the level of the RPA. The local packing effects due to short-range repulsions between the monomers and charge discreteness, which were also neglected in the theory, are another reason for that.

Fig. 7 shows experimental scattering results for the three structure factors. The decrease and gradual disappearance of the peaks in $G_{--}(q)$ and $G_{ch}(q)$ with addition of salt provides strong support for the view that the peaks arise from positional charge correlations. As discussed for the "salt-free" PEC data, samples prepared without exogenous salt contain < 0.6 mg NaCl. With addition of 0.8 mg NaCl, this implies a total mass of salt < 1.4 mg NaCl, and with addition of 2.0 mg NaCl, a total mass of NaCl $<$ 2.6 mg. The salt resistance for the samples presented here would be higher than that reported previously due to the difference in $c_{P,i}$. A faint correlation peak can still be observed with addition of 2.0 mg NaCl, which corresponds to $c_s \approx 0.74$ wt % (2.6 mg NaCl/352 mg PEC) exceeding the salt resistance previously reported, $c_s \approx 0.55$ wt % (52). Under these conditions, the Debye radius $r_D \approx 0.8$ nm remains higher than the polymer screening radius, $r_p \approx 0.5$ nm, so that $s < 1$ and the peak is indeed expected to survive. The exogenous salt added here, in amounts of 10 and 50 mg NaCl, is well above the salt resistance and provides $s > 1$, and therefore, all structure factors return to an OZ form. Above the salt resistance, a complete screening of Coulomb interactions results in a quasi-neutral semidilute solution.

The evolution of $G_{tot}(q)$ at increasing c_s is also consistent across theory, simulations, and experiments. Figs. 5*A* and 7*A* demonstrate that the plateau value of the OZ curve, which is equal to the osmotic compressibility of the PECs, Eq. **23**, decreases. The PEC compressibility is defined by the balance of excluded volume repulsions and Coulomb attractions. At a fixed polymer density, the addition of salt screens attractions but does not affect repulsions, leading to a decrease in PEC compressibility. The ratio between the $G_{tot}(q \to 0)$ plateau values for the salt-free and salted PECs is close to 3 in both experiments and simulations. The RPA predicts the same trend with a lower factor of 1.3

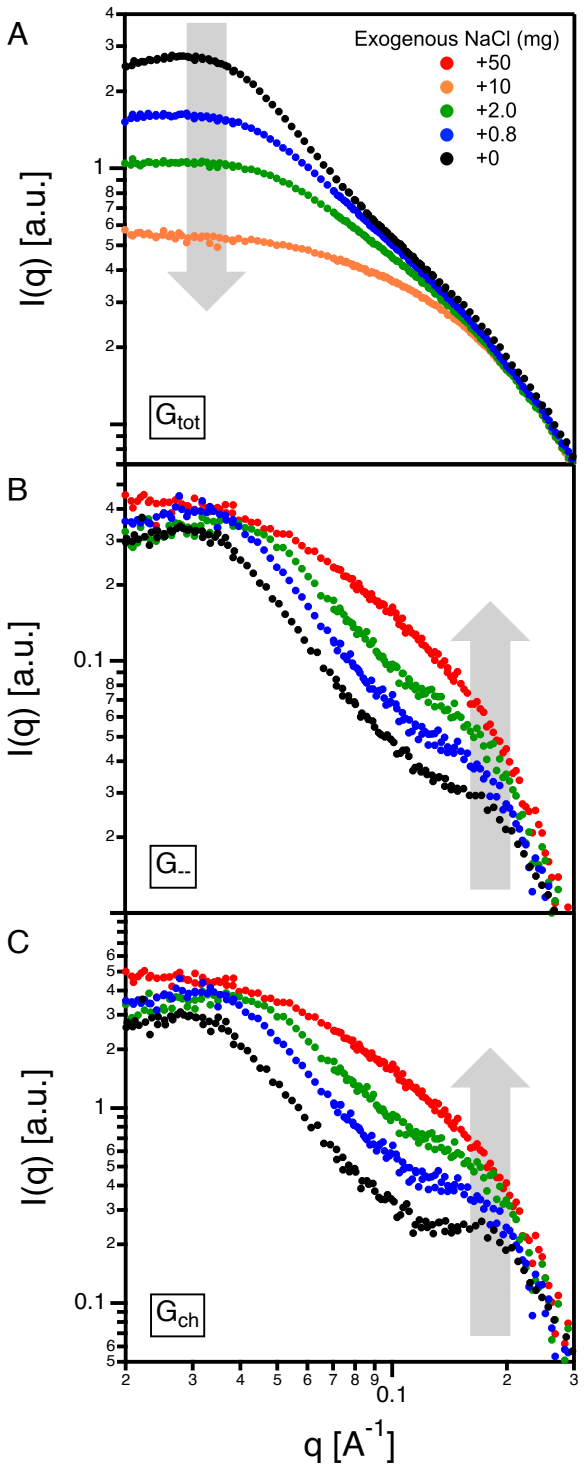

Fig. 7. Background-subtracted scattering intensity $I(q)$ as a function of wavevector q obtained from SANS experiments on salt-added PECs with the fraction $f = 0.30$ of ionic monomers. (*A*) G_{tot} is obtained via complexation of fully protonated chains of poly(Am_{ox}-*stat*-EO) and poly(Sulf-*stat*-EO) and measured against D_2O; (*B*) G_{--} is obtained via complexation of fully protonated poly(Sulf-*stat*-EO) and partially deuterated poly(Am_{ox}-*stat*-d_4-EO) and measured against $H_2O/D_2O = 49/51$ that contrast matches deuterated polycation; (*C*) G_{ch} is obtained by subtracting G_{tot} from G_{--} through the theoretical equation $G_{ch} = 4G_{--} - G_{tot}$ after their appropriate normalization at high q values.

for Θ solvent conditions, as follows from Eq. **21** (*SI Appendix*). This discrepancy can be primarily attributed to the applicability range of the virial expansion employed in the theory, $\phi \ll 1$, and the fact that the systems considered in our simulations are relatively dense, e.g., $\phi = c_p\sigma^3 \approx 0.388$. Indeed, if within the RPA, the solvent is assumed to be athermal, and two-body repulsions dominate over three-body, the factor of 1.3 changes to 4 (*SI Appendix*). It can also be seen in Figs. 5*A* and 7*A* that salt extends the scattering plateau in $G_{tot}(q)$ to higher q values. This is consistent with the theoretical predictions of Eqs. **21** and **22**, which suggest that ξ_E and the parameter t are decreasing functions of c_s and that the plateau's right edge, $q_E \simeq \xi^{-1}$, increases with c_s.

Relation to Microphase Separation Peak. The observed peak in $G_{ch}(q)$ is analogous to the scattering peak indicative of electrostatically stabilized microphase separation in a PEC phase. The latter has been predicted for PECs/blends of weakly and oppositely charged, chemically incompatible polyelectrolytes (29, 39–42) and was recently observed in SAXS experiments (57). The q-values of the charge correlation peak reported here and the peak indicative of microphase separation in PEC are predicted to coincide, $q^* = r_p^{-1}$, which reflects the closely related physics of the two phenomena (29). Theory suggests that the charge correlation peak continuously grows and sharpens as χ_{+-} increases, which indicates a strong increase of positional correlations between polyanions and polycations. At the spinodal, the RPA predicts the divergence of the charge structure factor (29), as microphase separation is a weak crystallization phase transition (58) from a liquid system with short-range correlations (considered here) to a system with long-range order. The structure factor divergence is corrected (39) when fluctuations are taken into account within the Brazovskii–Fredrickson–Helfand approach (36–38). Exogenous salt suppresses charge correlations in the system considered here as well as electrostatically stabilized microphases. The RPA predicts that the peak in $G_{ch}(q)$ disappears at the same (reduced) salt concentration, $s = 1$. For electrostatically stabilized microphases, this corresponds to the coordinate of the Lifshitz point where the system transitions from microphase to macrophase separation (29, 41, 42, 59).

Conclusions

We have provided direct experimental evidence in support of the existence of positional charge correlations in liquid polyelectrolyte complexes. Synthetic polyelectrolytes were carefully designed, and SANS measurements with contrast matching were performed to probe a long-standing theoretical picture. Oxyanionic copolymerization of allyl glycidyl ether with ethylene oxide or deuterated ethylene oxide provided well-defined neutral precursors to near-ideally random copolyelectrolytes with or without deuterium labeling and charge densities of $f \approx 0.3$. The total polymer structure factor, $G_{tot}(q)$, obtained by scattering from complexes of oppositely charged polyelectrolytes without deuterium labeling, is in good agreement with previously reported scattering profiles displaying an Ornstein–Zernike form. The polyanion structure factor, $G_{--}(q)$, accessed by contrast-matching solvent and deuterium-labeled polycations, exhibited a shoulder at $q^* \approx 0.2$ Å^{-1}. The experimental charge structure factor, $G_{ch}(q)$, was calculated by subtracting the appropriately normalized $G_{--}(q)$ from $G_{tot}(q)$. A clear peak emerged in $G_{ch}(q)$ at q^*, which is attributed to positional correlations between charged monomers of polyanions and polycations. The peak position is defined by the electrostatic screening radius from polyelectrolytes, which is found to equal $r_p = 1/q^* \approx 0.5$ nm.

As salt was added to PECs at constant polymer density, the correlation peaks in $G_{--}(q)$ and $G_{ch}(q)$ gradually disappeared, returning all scattering profiles to a simple Ornstein–Zernike shape. The correlation peaks and their salt-induced suppression were predicted by the RPA analysis and observed in accompanying coarse-grained simulations. While field theory (15, 16, 26–29, 32) provides a more accurate and detailed description of the positional charge correlations in PECs, they can be qualitatively interpreted using a scaling approach (49). If the PEC is viewed as a melt of oppositely charged electrostatic blobs of size $\xi \simeq \xi_e$, the idea of charge correlations suggests that each blob in the salt-free PEC is preferentially surrounded by oppositely charged blobs (11–13). These local positional correlations result in the peak in the charge structure factor, $G_{ch}(q)$, and, hence, in the polyanion structure factor, $G_{--}(q)$, at $q^* \simeq \xi^{-1} \simeq r_p^{-1}$. The estimate of the blob size as the half-period of oscillations in $G_{ch}(r)$ yields $\xi \approx D/2 = \sqrt{2}\pi r_p \approx 2.2$ nm. Addition of salt results in the screening of Coulomb interactions, thereby diminishing the preferential adjacency of oppositely charged blobs until the PEC structurally resembles a mixed semidilute solution of barely distinguishable, quasi-neutral polyanions and polycations. Collectively, our combined results from theory, simulations, and experiments make a strong case for the existence of positional charge correlations as a fundamental feature of polyelectrolyte complexes.

Data, Materials, and Software Availability. All data needed to evaluate the conclusions in the paper are presented in the paper and/or supporting information.

ACKNOWLEDGMENTS. This work was supported by the Department of Energy, Basic Energy Sciences, Division of Materials Science and Engineering. A portion of this research used resources at the Spallation Neutron Source, a DOE Office of Science User Facility operated by the Oak Ridge National Laboratory. We gratefully acknowledge Carrie Gao for her assistance during the neutron scattering experiments.

Author affiliations: [a]Pritzker School of Molecular Engineering, University of Chicago, Chicago, IL 60637; [b]Center for Molecular Engineering and Materials Science Division, Argonne National Laboratory, Lemont, IL 60439; [c]Department of Chemical and Biomolecular Engineering, North Carolina State University, Raleigh, NC 27695; [d]Department of Materials Science and Engineering, University of Florida, Gainesville, FL 32611; and [e]Neutron Scattering Division, Oak Ridge National Laboratory, Oak Ridge, TN 37831

Author contributions: A.M.R. and A.E.N. designed research; A.E.N. and Y.N.F. synthesized polyelectrolytes; Y.N.F. performed scattering experiments under the guidance of W.T.H.; H.L. performed computer simulations; A.M.R. performed theoretical calculations; M.V.T. and P.F.N. supervised experimental work; J.J.d.P. supervised computational work; and Y.N.F., A.M.R., A.E.N., H.L., W.T.H., P.F.N., M.V.T., and J.J.d.P. wrote the paper.

The authors declare no competing interest.

This article is a PNAS Direct Submission.

1. C. P. Brangwynne, P. Tompa, R. V. Pappu, Polymer physics of intracellular phase transitions. *Nat. Phys.* **11**, 899–904 (2015).
2. V. Yeong, E. G. Werth, L. M. Brown, A. C. Obermeyer, Formation of biomolecular condensates in bacteria by tuning protein electrostatics. *ACS Cent. Sci.* **6**, 2301–2310 (2020).
3. N. A. Yewdall, A. A. M. André, T. Lu, E. Spruijt, Coacervates as models of membraneless organelles. *Curr. Opin. Colloid Interface Sci.* **52**, 101416 (2021).
4. A. I. Oparin, *The Origin of Life* (The Macmillan Company, London, UK, 1938).
5. M. Li, X. Huang, T.-Y.D. Tang, S. Mann, Synthetic cellularity based on non-lipid micro-compartments and protocell models. *Curr. Opin. Chem. Biol.* **22**, 1–11 (2014).

6. R. R. Poudyal *et al*., Template-directed RNA polymerization and enhanced ribozyme catalysis inside membraneless compartments formed by coacervates. *Nat. Commun.* **10**, 490 (2019).
7. R. J. Stewart, C. S. Wang, H. Shao, Complex Coacervates as a foundation for synthetic underwater adhesives. *Adv. Colloid Interface Sci.* **167**, 85–93 (2011).
8. Q. Zhao *et al*., Underwater contact adhesion and microarchitecture in polyelectrolyte complexes actuated by solvent exchange. *Nat. Mater.* **15**, 407–412 (2016).
9. Z. Zhou *et al*., Targeted polyelectrolyte complex micelles treat vascular complications in vivo. *Proc. Natl. Acad. Sci. U.S.A.* **118**, e2114842118 (2021).
10. J. de Grooth, R. Oborný, J. Potreck, K. Nijmeijer, W.M. de Vos, The role of ionic strength and odd–even effects on the properties of polyelectrolyte multilayer nanofiltration membranes. *J. Membr. Sci.* **475**, 311–319 (2015).
11. N. P. Shusharina, E. B. Zhulina, A. V. Dobrynin, M. Rubinstein, Scaling theory of diblock polyampholyte solutions. *Macromolecules* **38**, 8870–8881 (2005).
12. A. M. Rumyantsev, E. B. Zhulina, O. V. Borisov, Complex coacervate of weakly charged polyelectrolytes: Diagram of states. *Macromolecules* **51**, 3788–3801 (2018).
13. M. Rubinstein, Q. Liao, S. Panyukov, Structure of liquid coacervates formed by oppositely charged polyelectrolytes. *Macromolecules* **51**, 9572–9588 (2018).
14. Z. Wang, M. Rubinstein, Regimes of conformational transitions of a diblock polyampholyte. *Macromolecules* **39**, 5897–5912 (2006).
15. V. Yu. Borue, I. Ya. Erukhimovich, A statistical theory of weakly charged polyelectrolytes: Fluctuations, equation of state and microphase separation. *Macromolecules* **21**, 3240–3249 (1988).
16. V. Yu. Borue, I. Ya. Erukhimovich, A statistical theory of globular polyelectrolyte complexes. *Macromolecules* **23**, 3625–3632 (1990).
17. J. Lee, Y. O. Popov, G. H. Fredrickson, Complex coacervation: A field theoretic simulation study of polyelectrolyte complexation. *J. Chem. Phys.* **128**, 224908 (2008).
18. K. T. Delaney, G. H. Fredrickson, Theory of polyelectrolyte complexation–Complex coacervates are self-coacervates. *J. Chem. Phys.* **146**, 224902 (2017).
19. K. Shen, Z.-G. Wang, Polyelectrolyte chain structure and solution phase behavior. *Macromolecules* **51**, 1706–1717 (2018).
20. P. G. de Gennes, *Scaling Concepts in Polymer Physics* (Cornell University Press, Ithaca, NY, 1979).
21. E. Spruijt *et al*., Structure and dynamics of polyelectrolyte complex coacervates studied by scattering of neutrons, X-Rays, and light. *Macromolecules* **46**, 4596–4605 (2013).
22. A. B. Marciel, S. Srivastava, M. V. Tirrell, Structure and rheology of polyelectrolyte complex coacervates. *Soft Matter* **14**, 2454–2464 (2018).
23. H. M. Fares *et al*., Scattering neutrons along the polyelectrolyte complex/coacervate continuum. *Macromolecules* **51**, 4945–4955 (2018).
24. M. Daoud *et al*., Solutions of flexible polymers. Neutron experiments and interpretation. *Macromolecules* **8**, 804–818 (1975).
25. J. P. Cotton *et al*., Experimental determination of the temperature-concentration diagram of flexible polymer solutions by neutron scattering. *J. Chem. Phys.* **65**, 1101–1108 (1976).
26. M. Castelnovo, J.-F. Joanny, Formation of polyelectrolyte multilayers. *Langmuir* **16**, 7524–7532 (2000).
27. A. Kudlay, M. Olvera de la Cruz, Precipitation of oppositely charged polyelectrolytes in salt solutions. *J. Chem. Phys.* **120**, 404–412 (2004).
28. J. Qin, J. J. de Pablo, Criticality and connectivity in macromolecular charge complexation. *Macromolecules* **49**, 8789–8800 (2016).
29. A. M. Rumyantsev, E. Yu. Kramarenko, O. V. Borisov, Microphase separation in complex coacervate due to incompatibility between polyanion and polycation. *Macromolecules* **51**, 6587–6601 (2018).
30. A. Yu. Grosberg, A. R. Khokhlov, *Statistical Physics of Macromolecules* (AIP Press, New York, NY, 1994).
31. A. R. Khokhlov, I. Y. Erukhimovich, A new class of systems exhibiting microphase separation: Polymer blends with a nonlocal entropy of mixing. *Macromolecules* **26**, 7195–7202 (1993).
32. A. M. Rumyantsev, I. I. Potemkin, Explicit description of complexation between oppositely charged polyelectrolytes as an advantage of the random phase approximation over the scaling approach. *Phys. Chem. Chem. Phys.* **19**, 27580–27592 (2017).
33. S. P. O. Danielsen, J. McCarty, J.-E. Shea, K. T. Delaney, G. H. Fredrickson, Small ion effects on self-coacervation phenomena in block polyampholytes. *J. Chem. Phys.* **151**, 034904 (2019).
34. G. H. Fredrickson, *The Equilibrium Theory of Inhomogeneous Polymers* (Clarendon Press, Oxford, UK, 2006).
35. M. Castelnovo, J.-F. Joanny, Complexation between oppositely charged polyelectrolytes: Beyond the random phase approximation. *Eur. Phys. J. E* **6**, 377–386 (2001).
36. S. A. Brazovskii, Phase transition of an isotropic system to a nonuniform state. *J. Exp. Theor. Phys.* **41**, 85–89 (1975).
37. G. H. Fredrickson, E. Helfand, Fluctuation effects in the theory of microphase separation in block copolymers. *J. Chem. Phys.* **87**, 697–705 (1987).
38. A. V. Dobrynin, I. Ya. Erukhimovich, Weak crystallization and structural phase transitions in weakly charged polyelectrolyte systems. *J. Exp. Theor. Phys.* **72**, 751–759 (1991).
39. A. M. Rumyantsev, J. J. de Pablo, Microphase separation in polyelectrolyte blends: Weak segregation theory and relation to nuclear "pasta". *Macromolecules* **53**, 1281–1292 (2020).
40. A. M. Rumyantsev, A. A. Gavrilov, E. Yu. Kramarenko, Electrostatically stabilized microphase separation in blends of oppositely charged polyelectrolytes. *Macromolecules* **52**, 7167–7174 (2019).
41. D. J. Grzetic, K. T. Delaney, G. Fredrickson, Electrostatic manipulation of phase behavior in immiscible charged polymer blends. *Macromolecules* **54**, 2604–2616 (2021).
42. A. V. Subbotin, A. N. Semenov, The structure of polyelectrolyte complex coacervates and multilayers. *Macromolecules* **54**, 1314–1328 (2021).
43. K. Kremer, G. S. Grest, Dynamics of entangled linear polymer melts: A molecular-dynamics simulation. *J. Chem. Phys.* **92**, 5057–5086 (1990).
44. G. S. Grest, M. Murat, Structure of grafted polymeric brushes in solvents of varying quality: A molecular dynamics study. *Macromolecules* **26**, 3108–3117 (1993).
45. W. M. Brown, A. Kohlmeyer, S. J. Plimpton, A. N. Tharrington, Implementing molecular dynamics on hybrid high performance computers-particle-particle particle-mesh. *Comput. Phys. Commun.* **183**, 449–459 (2012).
46. S. J. Plimpton, Fast parallel algorithms for short-range molecular dynamics. *J. Comput. Phys.* **117**, 1–19 (1995).
47. J.-M.Y. Carrillo, A. V. Dobrynin, Polyelectrolytes in salt solutions: Molecular dynamics simulations. *Macromolecules* **44**, 5798–5816 (2011).
48. A. R. Khokhlov, K. A. Khachaturian, On the theory of weakly charged polyelectrolytes. *Polymer* **23**, 1742–1750 (1982).
49. The oscillating profile of the charge-charge correlation function, $G_{ch}(r)$, is seemingly consistent with the coacervate blob structure. However, we are unaware of if/how this result can be derived (rather than a posteriori interpreted) within the scaling approach. For instance, the scaling derivation of even Eq. 9 for r_p suggest non-oscillating Debye-Hückel charge screening (12).
50. R. Sayko, Y. Tian, H. Liang, A. V. Dobrynin, Charged polymers: From polyelectrolyte solutions to polyelectrolyte complexes. *Macromolecules* **54**, 7183–7192 (2021).
51. M. Hans, H. Keul, M. Möller, Chain transfer reactions limit the molecular weight of polyglycidol prepared via alkali metal based initiating systems. *Polymer* **50**, 1103–1108 (2009).
52. A. E. Neitzel *et al*., Polyelectrolyte complex coacervation across a broad range of charge densities. *Macromolecules* **54**, 6878–6890 (2021).
53. W. T. Heller *et al*., The suite of small-angle neutron scattering instruments at Oak Ridge National Laboratory. *J. Appl. Crystallogr.* **51**, 242–248 (2018).
54. W. T. Heller *et al*., drtsans: The data reduction toolkit for small-angle neutron scattering at Oak Ridge National Laboratory. *SoftwareX* **19**, 101101 (2022).
55. G. D. Wignall, F. S. Bates, Absolute calibration of small-angle neutron scattering data. *J. Appl. Crystallogr.* **20**, 28–40 (1987).
56. L. Li *et al*., Phase behavior and salt partitioning in polyelectrolyte complex coacervates. *Macromolecules* **51**, 2988–2995 (2018).
57. M. L. Le *et al*., Electrostatic interactions control the nanostructure of conjugated polyelectrolyte-polymeric ionic liquid blends. *Macromolecules* **55**, 8321–8331 (2022).
58. E. I. Kats, V. V. Lebedev, A. R. Muratov, Weak crystallization theory. *Phys. Rep.* **228**, 1–91 (1993).
59. G. H. Fredrickson *et al*., Ionic compatibilization of polymers. *ACS Polym. Au* **2**, 299–312 (2022).